Efficient Solar-Driven Water Harvesting from Arid Air with Metal–Organic Frameworks Modified by Hygroscopic Salt

Jiaxing Xu[+], Tingxian Li[+],* Jingwei Chao, Si Wu, Taisen Yan, Wenchen Li, Biye Cao, and Ruzhu Wang*

Abstract: *Freshwater scarcity is a global challenge threatening human survival, especially for people living in arid regions. Sorption-based atmospheric water harvesting (AWH) is an appealing way to solve this problem. However, the state-of-the-art AWH technologies have poor water harvesting performance in arid climates owing to the low water sorption capacity of common sorbents under low humidity conditions. We report a high-performance composite sorbent for efficient water harvesting from arid air by confining hygroscopic salt in a metal–organic framework matrix (LiCl@MIL-101(Cr)). The composite sorbent shows $0.77\ g\,g^{-1}$ water sorption capacity at 1.2 kPa vapor pressure (30% relative humidity at 30°C) by integrating the multi-step sorption processes of salt chemisorption, deliquescence, and solution absorption. A highly efficient AWH prototype is demonstrated with LiCl@MIL-101(Cr) that can enable the harvesting of 0.45–0.7 kg water per kilogram of material under laboratory and outdoor ambient conditions powered by natural sunlight without optical concentration and additional energy input.*

Introduction

Freshwater scarcity is one of the great challenges worldwide.[1] According to a report from the World Health Organization (WHO), 2.1 billion people globally lack safe drinking water at home and 844 million people have no primary drinking water facility. To quench the thirst of the world, researchers have developed many water harvesting technologies, including desalination of seawater and rainwater collection. However, most regions suffering from water stress are landlocked and arid, where natural liquid water is inaccessible. Alternatively, the water source that is moisture and droplets in the air is considered enough to meet the needs of people living in arid regions. The amount of this water is estimated to be 12900 trillion liters, six times higher than that of the water in the world's rivers.[2] Direct water harvesting from fog, dew-water collection driven by chillers, and

sorption-based water capture using sorbent are three major strategies to realize atmospheric water harvesting (AWH).[3] Among them, the fog water collection technology is limited by strict requirements of high relative humidity (RH), whereas the dew-water collection technology requires tremendous energy consumption to cool down the air from ambient temperature to dew-point temperature in an arid climate.[4] In recent years, solar-enabled water-relative technologies have attracted much attention for economical sustainable water harvesting and purification,[5] therefore, solar-driven sorption-based AWH is an emerging technology for low-cost water harvesting from dry air.

According to the different cohesive forces between sorbents and water vapor, sorption interactions are commonly divided into physical sorption and chemical sorption. For most classic solid physical sorbents, such as the porous materials of silica gels and zeolites, the strong interaction of the sorbent with water molecules results in a high regeneration temperature ($T_{re} > 100°C$) and thus this process is difficult to power directly by natural sunlight. Chemical sorbents, such as hygroscopic salts, usually have higher water uptakes and lower regeneration temperatures for water harvesting than physical sorbents,[6] but can suffer from the serious drawbacks of corrosion, swelling, and agglomeration. As a result, the dramatic performance degradation of both water sorption capacity and sorption kinetics occurs after several sorption–desorption cycles.[7] To solve these problems, a family of selective water sorbents "composite salt in porous matrix" (CSPM) was proposed and adopted for sorption-based heating, cooling, and AWH, in which the porous matrix is used to solve the agglomeration and solution leakage of salts.[8,9] However, the salt contents of CSPMs are usually low because of the limitation of the low pore volumes of traditional porous matrices, such as silica gel, alumina, and porous carbon. Metal–organic frameworks (MOFs) with "S"-shaped water sorption isotherm behaviors (easily driven by small temperature and/or pressure changes) are possible alternatives to traditional atmospheric water harvesting materials.[10] The groups of Wang and Yaghi have demonstrated an atmospheric water harvesting device with MOF-801 in an arid climate powered by natural sunlight.[11] Later, the AWH device was scaled up from gram scale to kilogram scale and successfully achieved a water harvesting capacity of approximately 0.07 kg of water per kilogram of material at a desert region.[12] Recently, the low-cost MOF-303 was applied in a solar photovoltaic (PV) powered continuous water harvester, generating 0.7 kg of water per kilogram of MOF per day after several cycles.[13] On the other hand, some

[*] J. Xu,[+] Prof. T. Li,[+] J. Chao, S. Wu, T. Yan, W. Li, B. Cao, Prof. R. Wang
Research Center of Solar Power & Refrigeration, School of Mechanical Engineering, Shanghai Jiao Tong University
Shanghai 200240 (China)
E-mail: litx@sjtu.edu.cn
          rzwang@sjtu.edu.cn

[+] These authors contributed equally to this work.

Supporting information and the ORCID identification number(s) for the author(s) of this article can be found under:
https://doi.org/10.1002/anie.201915170.

macroporous hydrogels and aerogels with rich oxygenic functional groups show high potential for humidity-related applications, such as energy harvesting from moisture,[14] solar water desalination,[15] and AWH.[16] In comparison with MOFs, the preparation of these materials is relatively low-cost and easier, but these materials generally show low water capture capacity and slow sorption kinetics in arid climates (RH < 30%).

In recent years, research on new porous matrix materials with large pore volumes inspired the design and development of new composite sorbents to achieve high sorption capacity by filling with large amount of salts. Similar to the CSPMs, several composite sorbents of salt@matrix were reported to achieve high-performance AWH, of which CaCl₂@polyacrylamide showed 0.70 g g⁻¹ water sorption capacity at 1.1 kPa vapor pressure (35% RH at 25°C),[17] CaCl₂@alginate showed 1.0 g g⁻¹ water uptake at 1.0 kPa vapor pressure (26% RH at 28°C),[18] and chloride-doped polypyrrole@N-isopropylacrylamide showed 0.7 g g⁻¹ water sorption capacity at 0.8 kPa vapor pressure (30% RH at 25°C).[19] Although hydrogels can supply large pore volumes to encapsulate hygroscopic salts, they suffer from several drawbacks including serious swelling,[19] low specific surface area, and low mechanical strength.[20] Recently, a novel composite sorbent of LiCl@hollow carbon sphere was reported to achieve multiple water harvesting cycles per day.[21] Alternatively, porous MOF materials are an optimal choice as a porous matrix because of their large nanoscale pore volume, large specific surface area, robust pore structures, and tunable chemical features. Salt@MOF materials, such as CaCl₂@UiO-66 and CaCl₂@MIL-101(Cr), have been described by confining CaCl₂ in MOF matrices to achieve a sorption-based heat transformation, showing 0.67 g g⁻¹ and 0.60 g g⁻¹ water sorption capacity at 1.2 kPa vapor pressure (30% RH at 30°C).[22] However, the complicated multi-step sorption mechanisms of hygroscopic salts in these composite sorbents have not been analyzed, and the advanced heat design and energy analysis of AWH devices needs further investigation for efficient AWH practical applications.[23]

Herein, we firstly established that LiCl is the most promising inorganic salt for AWH in an arid climate by evaluating the water sorption performance of typical hygroscopic salts. Then, we selected a water-stable MOF, MIL-101(Cr) (Cr₃F(H₂O)₂O(BDC)₃) (BDC = 1,4-benzenedicarboxylate), as the porous matrix because of its extraordinary pore properties. Afterwards, we developed a novel composite sorbent by encapsulating LiCl in the MIL-101(Cr), named as LiCl@MIL-101(Cr). Attributing to the homogeneous nanoscale pore and large pore volume of MIL-101(Cr), the water capture/release process of nanoscale LiCl crystals occurs inside the cages of MOFs with faster water sorption kinetics, lower regeneration temperature, and excellent cycling stability than bulk LiCl. Furthermore, we revealed the multi-step sorption mechanisms of salt chemisorption, deliquescence, and solution absorption for water uptake of LiCl@MIL-101(Cr). Finally, we demonstrated a lab-scale water harvesting device for applications achieving 7.0 kg kg⁻¹ water harvesting per cycle under the laboratory conditions (standard one sun irradiation) and achieving 4.5 kg kg⁻¹ water harvest-

ing under natural sunlight (0.5–0.8 kW m⁻²). The proposed water harvesting device based on LiCl@MIL-101(Cr) can provide a feasible method to realize highly efficient AWH in arid regions powered by natural sunlight without optical concentration or additional energy input.

Results and Discussion

Working Principle of Sorption-Based AWH

For a typical semi-open AWH system, sorbents capture water from the air during the open phase at night and release water through desorption during the closed phase at daytime.[24] Therefore, the overall AWH performance depends on the water sorption–desorption performance of sorbents. To realize highly efficient water harvesting in an arid climate, the sorbent requires following characteristics: i) high water sorption capacity at low humidity (≤ 30% RH), ii) low regeneration temperature (< 100°C), iii) fast water sorption–desorption kinetics, and iv) good cycling stability. Herein, a Cr-based MOF, MIL-101(Cr), is selected as the porous matrix because of its large pore volume of 2.0 cm³ g⁻¹ allowing a high amount of salt loading, large specific surface area of 4100 m² g⁻¹ providing large reaction contact area,[25] suitable pore diameter of 2.9/3.3 nm for inducing nanoscale crystallization of LiCl, and robust pore structure with good cycling stability.[26] LiCl is selected as the active salt encapsulated inside the MOF because it has the highest water harvesting capacity among typical hygroscopic salts under arid AWH working conditions (1.2 kPa at 30°C for water sorption and 4.2 kPa at 80°C for water desorption) (see Figure S4). Two LiCl@MIL-101(Cr) composite sorbents with a low salt content of 33 wt% and a high salt content of 51 wt% were prepared, named as LiCl@MIL-101(Cr)_33 and LiCl@MIL-101(Cr)_51, respectively (Table S1).

This water sorption-desorption cycle is elaborated in the isosteric cycle diagram for a typical arid climate (see Figure 1b), together with theoretical water sorption equilibrium lines of dilute LiCl solutions, saturated solution, and LiCl crystal. The chemical reaction equilibrium of LiCl·H₂O dehydration can be expressed as Equation (1),[27]

$$\ln \frac{P_{vapor}}{P_0} = -\frac{8668.18}{(T + 273.15)} - 4\ln(T + 273.15) + 44.589 \qquad (1)$$

where the unit of water vapor pressure is kPa, and the unit of temperature is °C.

Before the water release and collection, the composite sorbent captures water from arid air at 1.2 kPa vapor pressure (30% RH at 30°C) and reaches its water sorption equilibrium at point A where the LiCl solution concentration is 37%. This finding indicates that a LiCl solution with a concentration below 37% is desirable during the sorbent preparation process to avoid solution leakage in working process. During the water desorption process, the sorbent is heated from point A to point B and releases a small amount of water to make the vapor pressure of the device increase from its water sorption pressure of 1.2 kPa to a saturated pressure of 4.2 kPa for
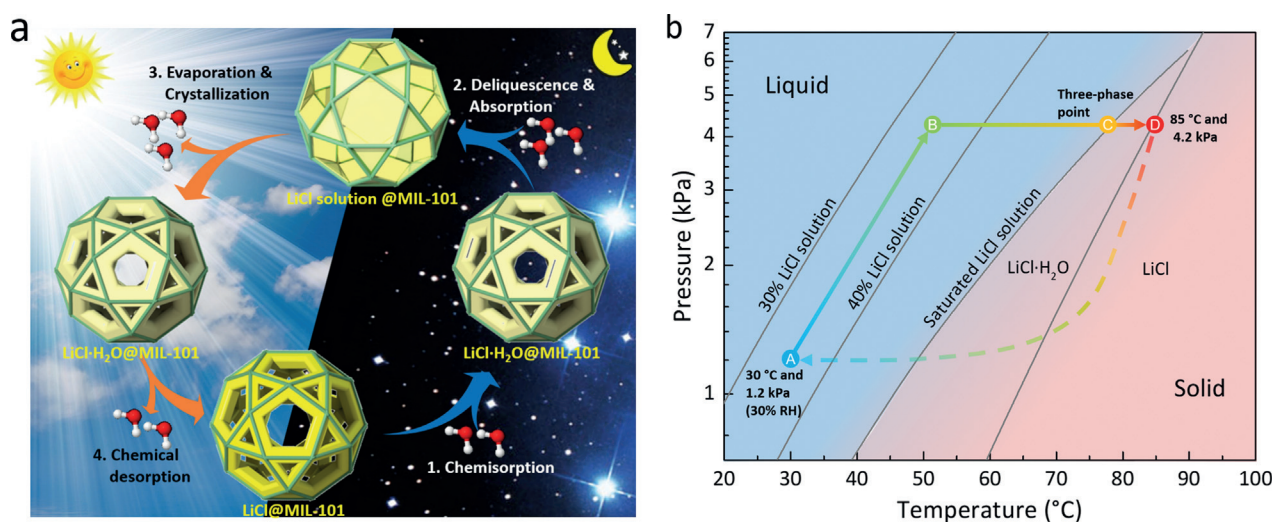
Figure 1. Working principle of sorption-based AWH using LiCl@MIL-101(Cr) composite sorbents. a) Schematic of the multi-step water sorption/desorption processes of LiCl@MIL-101(Cr). The green frameworks of spheres represent cages of MIL-101(Cr) and the yellow parts represent LiCl, LiCl·H_2O, or LiCl solution. Solid chemisorption, solid–liquid deliquescence, and liquid absorption processes during the water sorption phase at night and liquid evaporation, liquid–solid crystallization, and solid chemical desorption during the water harvesting phase in the daytime are shown. b) Isosteric cycle states of the multi-step three-phase processes of LiCl during water sorption–desorption steps: A–B, preheating process; B–C, evaporation of LiCl solution and three-phase stage crossing point C from the left side (liquid state) to the right side (solid state); C–D, crystallization of LiCl·H_2O and chemical desorption of LiCl·H_2O crossing point D from the left side to the right side; D–A, water capture from ambient air by solid chemisorption, solid–liquid deliquescence, and liquid absorption processes. Point A represents the typical water capture conditions in arid regions of 30°C and 1.2 kPa vapor pressure (30% RH at 30°C), where LiCl exists as 37% LiCl solution. Point D represents the general water release conditions of 85°C and 4.2 kPa vapor pressure, where LiCl exists as an anhydrous salt crystal.

water condensation at 30°C. Then, the water continuously evaporates from dilute solution on increasing the temperature of the salt solution (from point B to point C), and the pressure remains stable at 4.2 kPa, controlled by a stable condensation temperature of 30°C. Once the sorbent temperature is higher than the equilibrium temperature of three-phase point C (78°C), the liquid LiCl solution will crystalize to become solid LiCl·H_2O. Afterwards, if the heating temperature is further increased to be higher than that of point D (85°C), the coordination bond between water and LiCl will rupture and the last mole of water will be released from LiCl·H_2O to generate anhydrous LiCl (see Figure S5). This cycle shows the reversible multi-step three-phase sorption–desorption processes of AWH using LiCl. The solid chemical sorption–desorption, solid–liquid deliquescence/crystallization, and liquid absorption/evaporation of LiCl results in a large water capture–release potential from a relatively small temperature change of between 30 and 85°C.

Design and Characterization of LiCl@MIL-101(Cr)

The synthesis and morphologic characterization of LiCl@-MIL-101(Cr) composite sorbent is shown in Figure 2. The novel composite sorbent is synthesized by a post-synthesis method as shown in Figure 2a (see details in the Supporting Information). Firstly, pure MIL-101(Cr) is prepared by the hydrothermal reaction method.[30] Then, LiCl is added into the MIL-101(Cr) suspension with stirring overnight to allow chloride and lithium ions to infiltrate into the cages of MIL-101(Cr). The excess LiCl solution outside of MIL-101(Cr) is

removed by centrifugation, followed by a surface washing to remove excess LiCl solution adhered onto the external surface of MIL-101(Cr). After heating at 100°C, the anhydrous LiCl@MIL-101(Cr) composite sorbent is obtained. The prepared pure MIL-101(Cr) matrix exists as a micrometer-scale crystal aggregation (see SEM image in Figure 2b) and is composed of an ordered nanopore structure (see TEM image in Figure 2c). The SEM image of the LiCl@MIL-101(Cr) composite sorbent shows that the active LiCl is well encapsulated inside the cages of the MIL-101(Cr) matrix and there are a large number of interspaces among crystal aggregations of MIL-101(Cr) (see Figure 2d). After encapsulation of the salts into the cage of MIL-101(Cr), most pores of the MIL-101(Cr) matrix are occupied by LiCl and only a few pores can be seen in the TEM image (see Figure 2e). Elemental-distribution mapping with energy-dispersive X-ray spectrometry (EDX) reveals the uniform distribution of LiCl in the composite sorbent (see SEM–EDX image in Figure 2f and TEM–EDX image in Figure S6).

Powder X-ray diffraction (PXRD) patterns show that the composite sorbent with a low salt content of 33 wt% (LiCl@MIL-101(Cr)_33) has no additional peak characteristic of LiCl or LiCl·H_2O, indicating that LiCl is nearly completely confined inside the pores (see Figure S7). However, the composite sorbent with a high salt content of 51 wt% (LiCl@MIL-101(Cr)_51) has apparent LiCl peaks, which shows that some salt adheres on the external surface of MIL-101(Cr) (see Figure S7). Moreover, the addition of LiCl improves the hydrophilicity of MIL-101(Cr) (see Figure S8). The nitrogen gas adsorption isotherm shows that the LiCl@-MIL-101(Cr) composite sorbent has a Brunauer–Emmett–
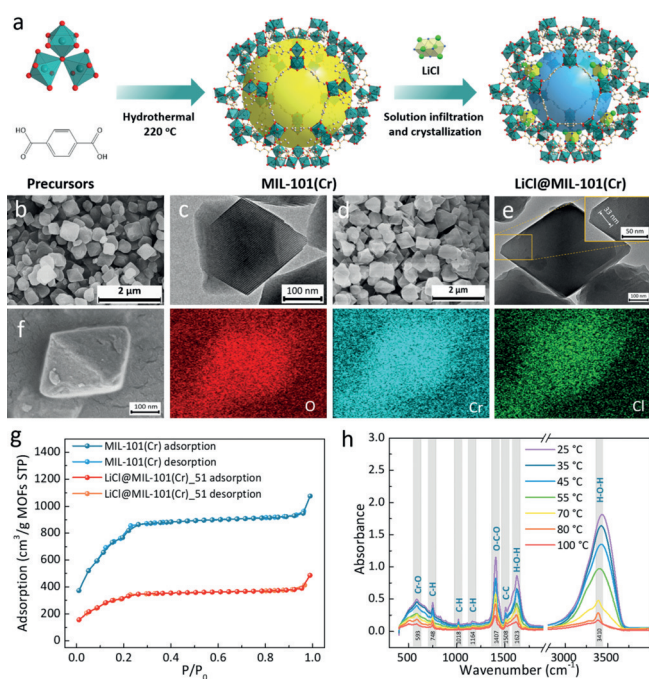
Figure 2. Synthesis and morphologic characterization of LiCl@MIL-101(Cr) composite sorbent. a) Schematic illustration of the fabrication process of LiCl@MIL-101(Cr). Dark cyan polyhedral, Cr; red, O; grey, C; blue, Li; green, Cl. b) SEM image of pure MIL-101(Cr). c) TEM image of pure MIL-101(Cr). d) SEM image of LiCl@MIL-101(Cr). e) TEM image of LiCl@MIL-101(Cr). f) Elemental mapping with EDX showing the homogeneous distribution of LiCl in MIL-101(Cr) matrix. g) N_2 gas adsorption–desorption isotherms of MIL-101(Cr) and LiCl@MIL-101(Cr)_51 at 77 K. h) Variable-temperature FTIR patterns of LiCl@MIL-101(Cr)_51 under different temperatures with a vapor pressure of 2.3 kPa.

Teller (BET) surface area as high as 1179 m² per gram MOFs and a large Barrett–Joyner–Halenda (BJH) pore volume of 0.69 cm³ per gram MOFs even at a high salt content of 51 wt% (see Figure 2g). The BET and BJH values of the pure MIL-101(Cr) matrix are 3311 $m^2 g^{-1}$ and 1.71 $cm^3 g^{-1}$, respectively, indicating that approximately 60% of the pore space of the MIL-101(Cr) matrix is occupied by LiCl and 40% of the space remains to allow mass transfer and storage of water during the AWH process. Therefore, although some salt adhered onto the external surface of the MOF, the majority of the water sorption process occurs inside the pores and the captured liquid water can be stored in the MOF matrix without leakage under AWH conditions (see ESEM images in Figure S9, optical images in Figure S10, and dynamic water sorption in Video S1). Moreover, variable-temperature Fourier transform infrared spectroscopy (FTIR) shows the chemical bonds of MIL-101(Cr) and hydrogen bonds of water in LiCl@MIL-101(Cr) (see Figure 2h). The chemical bonds in the composite sorbent correspond to those in the pure MOF (see Figure S11), confirming that there is no chemical interaction between MIL-101(Cr) and LiCl in the composite sorbent. The higher intensity of the bands corresponding to hydrogen bonding of the composite sorbent indicates a higher water sorption capacity than that of pure MIL-101(Cr). The disappearance of the band corresponding to the coordinated

water of MIL-101(Cr) for the composite sorbent (band at 3600 cm⁻¹) reveals that the LiCl crystallized near metal-ion clusters during the post-synthesis process.

Evaluation of Water Vapor Sorption Performance

The water sorption–desorption isotherms, water sorption–desorption isobars, water sorption kinetics, and water sorption/desorption cycling stability of the LiCl@MIL-101-(Cr) composite sorbent are shown in Figure 3. Firstly, the water sorption isotherms of pure MIL-101(Cr) and LiCl@MIL-101(Cr) composite sorbents were compared to optimize the amount of salt content in the LiCl@MIL-101(Cr) composite sorbent. Pure MIL-101(Cr) has an "S-shaped" sorption isotherm and an inflection of water uptake appears during the relative pressure ranging from 40 to 50% RH (see Figure 3a). This finding suggests that pure MIL-101(Cr) is not suitable for AWH in arid climates (≤30% RH) because of its very low water uptake. On the contrary, the LiCl@MIL-101(Cr) composite sorbent shows high water uptake under AWH conditions. Higher salt content is desirable for the composite sorbent but brings the risk of solution leakage during the water sorption process. Therefore, the common challenge of preparing a composite sorbent is to achieve optimal salt content. The LiCl@MIL-101(Cr) composite sorbent with low salt content (e.g. LiCl@MIL-101(Cr)_33) displays an ordinary water uptake under AWH conditions (≈0.3 g g⁻¹ at 30% RH) and the large pore volume of the MIL-101(Cr) matrix is not fully utilized at low RH, and it makes a positive contribution to water uptake until the RH reaches 40%. The salt content is majorly dependent on the concentration of the salt solution, therefore, the optimal solution concentration can be determined according to the water sorption equilibrium characteristics of LiCl as shown in Figure 1b. The composite sorbent with a salt content of 51% was synthesized by using the salt solution with a concentration of 37%. To avoid solution leakage, we have provided a guideline for the preparation of LiCl@MIL-101(Cr) with suitable salt contents under different humidity conditions (see Figure S12). LiCl@-MIL-101(Cr)_51 shows a high sorption capacity of 0.77 g g⁻¹ under AWH conditions (30% RH at 30°C), approximately 15 times higher than that of pure MIL-101(Cr), where all of the pores of the MOFs matrix are fully occupied by water without any solution leakage (see optical images in Figure S10, and dynamic water sorption in Video S1).

Pure LiCl shows much higher equilibrium water uptake than the composite sorbents, however, it suffers from slow water sorption kinetics and poor cycling stability, thus limiting direct applications in AWH. Moreover, pure LiCl powders would become bulk agglomerated crystals after several sorption cycles, and even lose water sorption capacity because of the very low mass transfer. The LiCl@MIL-101(Cr) composite sorbent shows faster water sorption kinetics than bulk LiCl during the water capture and release processes because of the mass-transfer enhancement by the high-porosity MOF matrix (see Figure 3b). This finding is further confirmed by comparison of the sorption kinetics of the composite sorbent with pure LiCl with different thicknesses
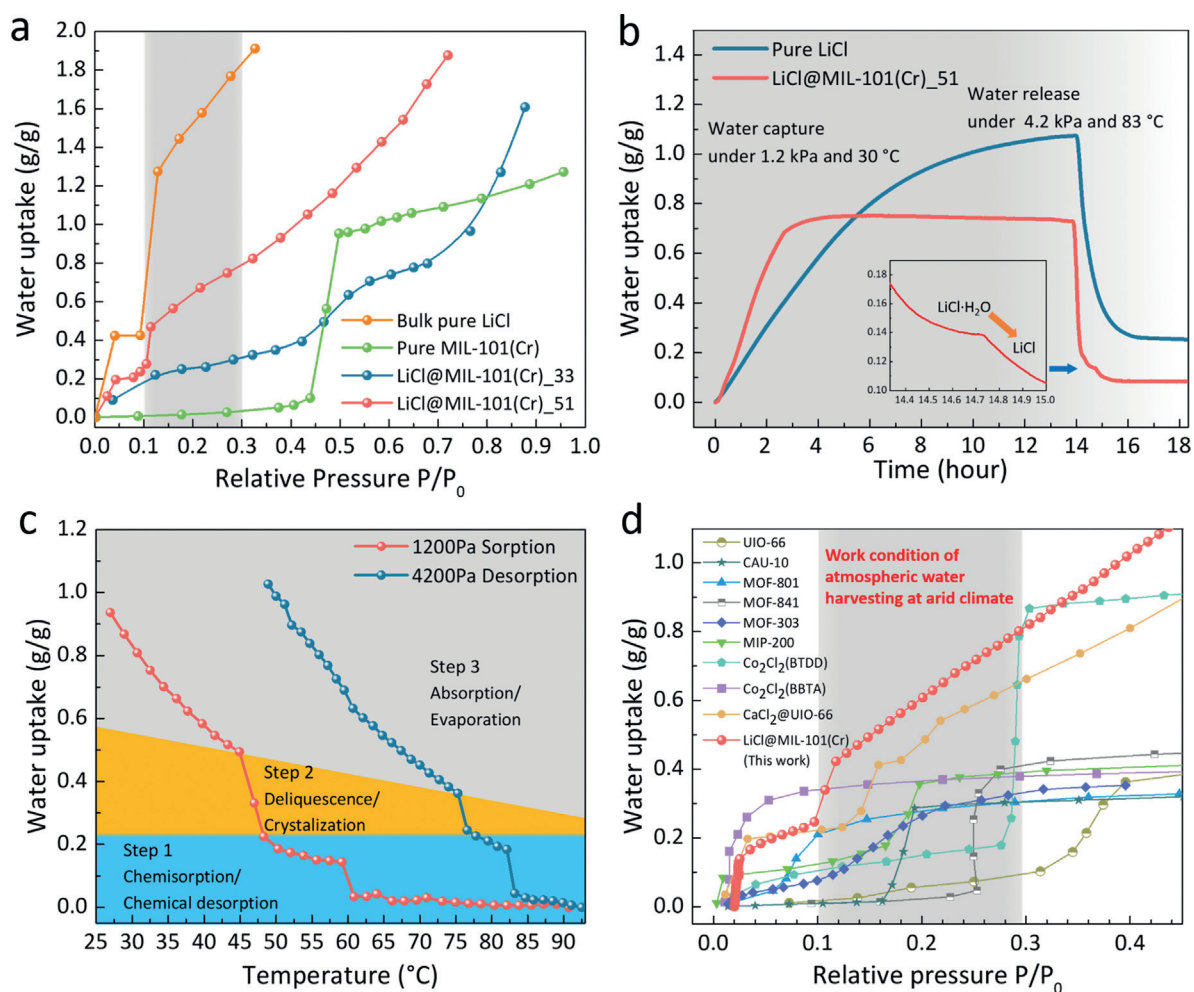
Figure 3. Water vapor sorption performance of LiCl@MIL-101(Cr) composite sorbent. a) Water sorption–desorption isotherms of pure MIL-101(Cr) and LiCl@MIL-101(Cr) with different salt contents of 33 and 51 wt% at 30°C. b) Dynamic water sorption–desorption of pure LiCl and LiCl@MIL-101(Cr)_51 at 1.2 kPa/30°C and 4.2 kPa/83°C. c) Water sorption–desorption isobars at 1.2 and 4.2 kPa vapor pressure showing multistep desorption processes during water release phase. Step 1: water sorption capacity slowly decreasing as result of the evaporation of LiCl solution with increasing temperature from room temperature to 76°C; Step 2: water sorption capacity sharply decreasing caused by the crystallization of LiCl·H_2O at 76°C; Step 3: water sorption capacity sharply decreasing owing to the chemical desorption of LiCl·H_2O at 83°C. The sorption–desorption isobars can be used to provide a guideline on the different cycled sorption capacities of LiCl@MIL-101(Cr) at different constraining temperatures. d) Comparison of water sorption capacities of MOFs and MOF-based composite sorbent.

(see Figure S13 and Table S2). Moreover, the effects of packing density on the water sorption kinetics are also investigated, and the results show that the sorption kinetics of the composite sorbent become slow when its packing density is higher than 1.2 g cm^{-3} (see Figure S14). FR-SEM images show that the composite sorbent can keep a stable structure before and after many cycles of AWH in an arid climate (see Figure S15), and it maintains high water sorption capacity and fast sorption kinetics after many repeated sorption–desorption cycles (see Figure S16). Thus, the composite sorbent is able to achieve several AWH cycles in one day, with the aim of improving the amount of water harvesting from air, because it can reach sorption equilibrium within 3 hours and release water within 1 hour.

Furthermore, the water sorption/desorption isotherms of the LiCl@MIL-101(Cr) composite sorbent show that it has the distinct advantage of integrating the multi-step sorption processes of salt chemisorption, deliquescence, and solution

absorption at different water vapor pressures (see Figure S17). Figure 3c shows the water sorption isobar of LiCl@MIL-101(Cr) at 1.2 kPa and its water desorption isobar at 4.2 kPa. The water release process for AWH applications can be regarded as quasi-equilibrium isobaric processes controlled by stable condensation pressure and temperature. Accordingly, the maximum water harvesting capacity is predicted to be as high as 0.77 g g^{-1} under typical arid working conditions (30% RH at 30°C). We observed that two inflection points of water sorption–desorption occur at 0.22 and 0.50 g g^{-1}, respectively, for both water sorption/desorption isotherms and isobars, corresponding to the chemical sorption/desorption, deliquescence/crystallization, and absorption/evaporation of the multi-step water sorption/desorption processes. Moreover, the dynamic water sorption at stepwise humidity conditions also confirmed the multi-step sorption mechanism of LiCl@MIL-101(Cr) under low and high humidity conditions (see Figure S18). The chemisorption

of LiCl has faster sorption kinetics than that of deliquescence and absorption, and the water harvesting contribution by water absorption of LiCl solution becomes large with increasing humidity, whereas the chemisorption of LiCl and the deliquescence of LiCl·H$_2$O remain almost constant.

The absorption/evaporation process makes a greater contribution to the water uptake of the composite sorbent at 4200 Pa vapor pressure than that at 1200 Pa vapor pressure owing to the higher solubility of LiCl in water at higher temperature. Moreover, we found that the reaction enthalpy of LiCl@MIL-101(Cr) during the water hydration–dehydration process varies nonlinearly with water uptake and it is approximately 45–65 kJ per mole of water (see Figure S19). The LiCl@MIL-101(Cr) composite sorbent has slight adsorption–desorption hysteresis for water capture and water release at different operating conditions (see Figure S20 and Figure S21). In addition, we provide the water sorption isotherms of LiCl@MIL-101(Cr) at different pressures and temperatures for the evaluation of AWH performance in different arid regions (see Figure S22).

We also found that the chemical desorption temperature of LiCl·H$_2$O slightly reduces from 85 to 83 °C when it is encapsulated in a MIL-101(Cr) matrix by comparing the equilibrium temperature of bulk LiCl·H$_2$O (see Figure 1b) with the chemical desorption temperature of LiCl@MIL-101(Cr)_51 (see Figure 3c). On the contrary, the chemical desorption temperatures of the composite sorbents of Ca-(NO$_3$)$_2$@Silica gel and CaCl$_2$@SBA-15 are reported to be higher than those of the bulk salts owing to the increase of the surface energy of the salt crystals.[28] To confirm this unusual finding, we measured and compared the water vapor sorption–desorption isobars of pure LiCl and composite sorbent (see Figure S23), and found that pure LiCl has large sorption–desorption hysteresis and its deliquescence/crystallization process simultaneous occurs with chemical sorption/desorption reactions. The thermogravimetric (TG) curves show that the dehydration temperature of chemical desorption for pure LiCl·H$_2$O becomes much higher when the crystallization process of LiCl simultaneously occurs. This is because the crystallization process firstly starts at the surface to generate a compact solid surface layer and thus makes the dehydration kinetics much slower, appearing as the increase of dehydration temperature (see Figure S24). On the contrary, the crystallization of LiCl inside MIL-101(Cr) becomes easier and results in fast dehydration kinetics and low regeneration temperature. To the best of our knowledge, the developed LiCl@MIL-101(Cr) composite sorbent shows higher water uptake capacity than other recently reported water sorption MOFs and MOF-based composite sorbents under arid AWH conditions (see Figure 3d).[11,29] These indications confirm that LiCl@MIL-101(Cr) composite sorbent is a potential candidate for achieving highly efficient AWH owing to its distinct advantages of high water sorption capacity at low humidity, relatively low desorption temperature, fast water sorption–desorption kinetics, and good cycling stability. Additionally, because the price of the Cr-based MOF is relatively cheap (see costs comparison in Table S4), the composite sorbent shows promising potential for large-scale AWH applications.

Demonstration of Atmospheric Water Harvesting

Atmospheric water harvesting from arid air under laboratory conditions powered by one sun irradiation is demonstrated in Figure 4. An all-in-one lab-scale water harvesting device is designed (see Figure 4a) and the composite sorbent is treated by carbon black as a light-absorbing layer to improve light-absorbance performance (see details in the Supporting Information). The LiCl@MIL-101(Cr)-C composite sorbent has a high light absorbance of approximately 96–98 %, and thus the heat-collection temperature is improved, but this material displays slightly lower sorption kinetics (see Figures S25–S27). Considering the effects of packing density on the water sorption kinetics (see Figure S14), the loose composite sorbent powder was directly put onto the polystyrene foam with a low packing density of 0.6 g cm^{-3}. The thermal conductivity of the composite sorbent is relatively low (see Figure S28 and S29), therefore, the packing thickness was limited at 2 mm to assure fast mass and heat transfer inside the composite sorbent. The dynamic water capture-release tests show that the composite sorbent has faster water sorption kinetics than the pure salt and it can reach sorption equilibrium within 10 hours in a constant temperature and humidity chamber under arid working conditions of 30 % RH at 30 °C without forced air convection (see Figure S30). Moreover, we found that there is no leakage of salt solution after overnight water vapor sorption, indicating the MOFs matrix can totally retain salt solution under these conditions (see optical photos in Figure 4a and ESEM images in Figure S9). The dynamic water harvesting process is observed by optical microscope (see Video S2) and the amount of water captured from the air is recorded by a weighting sensor.

During the water release and collection phase, the device is sealed and exposed to a solar simulator with 1 kW m^{-2} radiant fluxes (see Figure S31) to heat the sorbent from room temperature to its desorption temperature. The dilute LiCl solution firstly desorbs water vapor and causes the increase of air humidity near the sorbent (see Figure 4b). Owing to the occurrence of the vapor pressure difference between the air near the samples and the air near the condenser, the humidified moisture flows from the top to the bottom of the device. Concomitantly, the humidity of the air near the condenser rapidly increases from room humidity (point 1) to saturated condensation pressure (point 3, see blue line in Figure 4b). With the light heating, the temperature of sorbent increases quickly from 30 °C (point 1) to 97 °C (point 2, see red line in Figure 4b), whereas the condensation temperature increases slightly (≈3 °C) as shown in Figure 4c, indicating that the heat-dissipation power is enough to cool down the hot moist air to room temperature at this stage (see detailed condenser structure and energy analysis in Figure S32). The difference in vapor pressure between the air near the sorbent (see red line in Figure 4d) and the air near the condenser (see blue line in Figure 4d) becomes large and drives the moistures to quickly flow from the top to the bottom of the device (see Figure 4d), resulting in the fast condensation of water vapor.
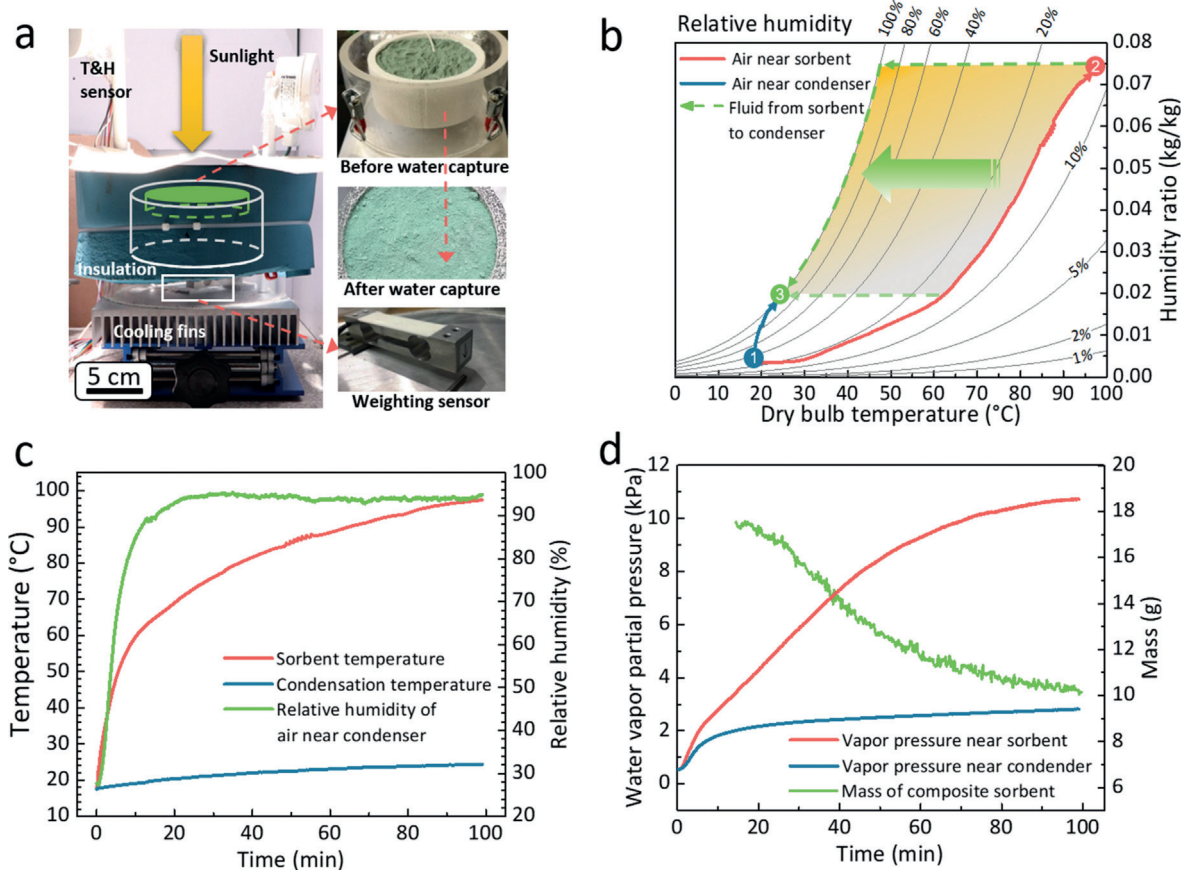
Figure 4. Atmospheric water harvesting under laboratory conditions powered by one sun irradiation. a) Photos of the AWH prototype with LiCl@MIL-101(Cr)-C composite sorbent, showing the structure of the all-in-one lab-scale water harvesting device and the color change of sorbent before and after water capture. b) Psychrometric chart showing the recorded state change of air during water release-condensation processes: 1–2, air near the sorbent heated from room temperature to water desorption temperature; 2–3, air flowing from sorbent to condenser driven by pressure difference together with temperature decrease and condensation occurrence. 1–3, air near the condenser humidified from arid state to saturated state with slight temperature increase. c) Representative temperature profiles for composite sorbent temperature, condenser temperature, and relative humidity of air near the condenser over time. d) Mass of sorbent over time and vapor pressure of air near the sorbent and condenser over time, showing AWH capacity as high as 0.7 kg kg^{-1} under one sun irradiation. A movie showing water collection process is provided in Video S2.

The heating temperature (95 °C) is higher than the chemical desorption temperature of LiCl·H$_2$O (85 °C) under the solar simulator (1 kW m^{-2}), therefore, the composite sorbent can thoroughly release all captured water to become anhydrous LiCl@MIL-101(Cr)-C. Efficient AWH of 0.70 kg kg^{-1} materials within 100 minutes is achieved, which is much higher than other reported lab-scale AWH devices (usually < 0.4 kg$_{water}$/kg$_{sorbent}$).[11]

We also performed outdoor experiments with the lab-scale AWH device for water collection in December 17, 2018, on a rooftop at the campus of Shanghai Jiao Tong University (SJTU) to validate the feasibility of the proposed AWH device based on the LiCl@MIL-101(Cr)-C composite sorbent (see photo in Figure S31). The local climate in Shanghai is moist all year round and it was impracticable to achieve the typical arid conditions for water vapor sorption in outdoor experiments (see Figure S33). Thus, we used a constant humidity chamber to simulate the arid climate (30 % RH at 30 °C) and performed the water sorption overnight inside the chamber. Then, we moved the water harvesting device to the

outdoor location to perform the water harvesting experiment. The device was closed and exposed under practical solar irradiance without optical concentration. The water release–condensation started within 30 minutes and finished within 180 minutes as shown by photos taken at different operating times (see Figure 5a), wherein most of the water condensation occurs from the 11:30 to 13:00 time points. The sorbent temperature sharply increases from ambient temperature to 70 °C with heating by solar flux varying between 0.6 and 0.8 kW m^{-2} (see Figure 5b). The water released by the composite sorbent causes an increase of the partial pressure of water vapor in the air near the sorbent, and the mass change of the composite sorbent before and after water release is used to calculate the amount of water harvested from the air (see Figure 5c). The driving temperature is not high enough for the chemical desorption of LiCl·H$_2$O, therefore, the experimental result is slightly lower than the predicted value from the water sorption isobars of the composite sorbent (see Figure 3d). The AWH device collected 4.5 g water by using 10 g sorbent within 90 minutes in the
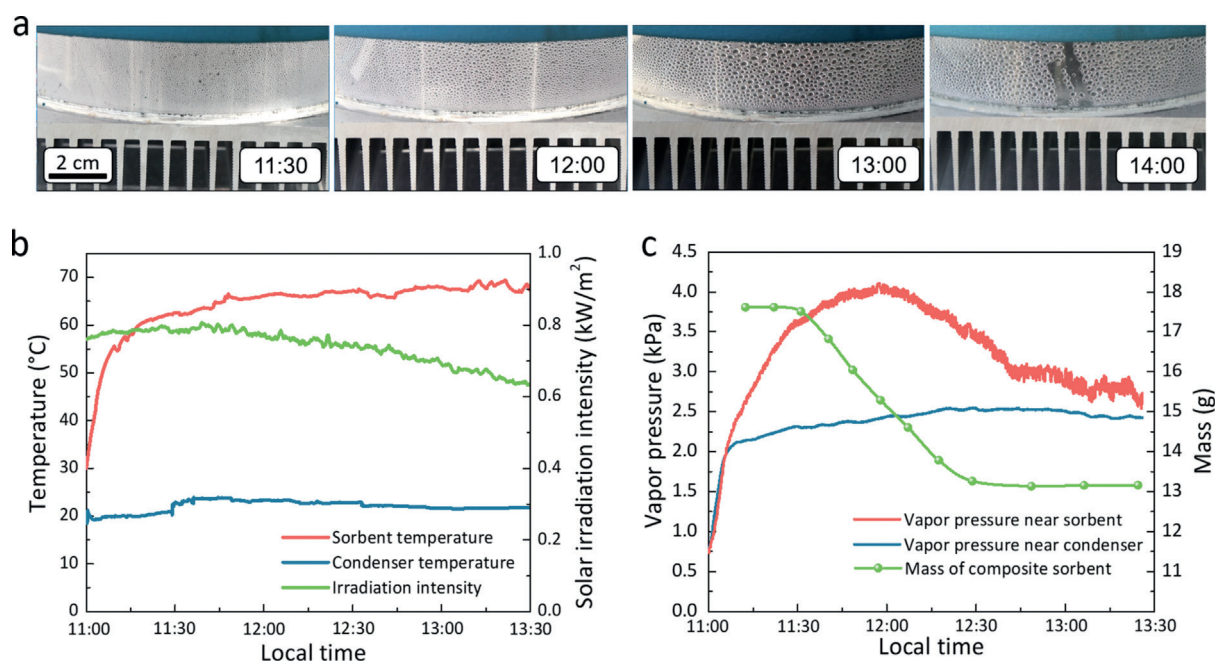
Figure 5. Atmospheric water harvesting under practical solar irradiation. a) Optical images of the surface of the water harvesting device at different times during the water collection process. b) Representative temperature profiles for sorbent temperature, condenser temperature, and solar irradiation intensity over time. c) Mass of sorbent over time and vapor pressure of air near the sorbent and condenser over time. A movie showing water collection process is provided in Video S3.

outdoor experiments, realizing $0.45\ kg\,kg^{-1}$ and $0.40\ L\,m^{-2}$ water harvesting capacity per cycle under arid water sorption conditions (30% RH at 30°C) and solar-driven desorption conditions (70°C and 3.7 kPa vapor pressure) without optical concentration. Further analysis of the energy balance and heat flux of the AWH device was performed. The average heat loss by heat radiation to the sky was $121.9\ W\,m^{-2}$ and the average heat loss by heat convection to the air was $191.7\ W\,m^{-2}$. The photothermal conversion efficiency was as high as 42.7% at the average solar flux of $719\ W\,m^{-2}$ (see detailed analysis in the Supporting Information and Figures S34,35). The quality of collected water by this lab-scale AWH device is examined by measuring the concentrations of primary ions with ICP-OES and ion chromatography (see Table S3 and Table S4), and the results show that the collected water reaches the guided drinking-water quality by the WHO.[30]

Conclusion

In summary, LiCl was found to be the most promising candidate of typical hygroscopic salts for atmospheric water harvesting (AWH) in arid climates. To solve the issues of low water sorption kinetics, high water desorption temperature, and poor cycling stability, we developed a novel composite sorbent by confining LiCl inside a porous metal-organic framework (MOF) matrix of MIL-101(Cr). Benefiting from the integration of the multi-step three-phase sorption processes of solid salt chemisorption, solid–liquid deliquescence, and liquid solution absorption, the LiCl@MIL-101(Cr) composite sorbent has the distinct advantage of a high water

sorption capacity at low humidity. The nanoscale pores of the MIL-101(Cr) matrix can provide enough space for water storage and induce nanoscale LiCl crystals with fast water sorption/desorption kinetics, relatively low regeneration temperature, and excellent cycling stability. The composite sorbent exhibits a high water sorption capacity of $0.77\ g\,g^{-1}$ under typical arid working conditions (30% RH at 30°C). To our knowledge, this is the highest value among reported MOFs and MOF-based composite sorbents for AWH under arid working conditions. We further demonstrated a lab-scale AWH device with LiCl@MIL-101(Cr) capable of high AWH performance with $0.70\ kg\,kg^{-1}$ materials under laboratory conditions $(1.0\ kW\,m^{-2})$ and $0.45\ kg\,kg^{-1}$ under outdoor natural sunlight conditions $(0.5$–$0.8\ kW\,m^{-2})$, together with a short water collection duration of within 100 minutes. This demonstration suggests that a solar-driven water harvesting device based on the LiCl@MIL-101(Cr) composite sorbent is a promising way to solve water scarcity in arid regions powered by natural sunlight without additional energy input.

Conflict of interest

The authors declare no conflict of interest.

[1] M. M. Mekonnen, A. Y. Hoekstra, *Sci. Adv.* **2016**, *2*, e1500323.

[2] B. Halford, *C&EN Global Enterprise* **2018**, *96*, 27–30.

[3] Y. Tu, R. Wang, Y. Zhang, J. Wang, *Joule* **2018**, *2*, 1452–1475.

[4] R. V. Wahlgren, *Water Res.* **2001**, *35*, 1–22.

[5] Y. Yang, X. Yang, L. Fu, M. Zou, A. Cao, Y. Du, Q. Yuan, C.-H. Yan, *ACS Energy Lett.* **2018**, *3*, 1165–1171.

[6] a) R. Li, Y. Shi, L. Shi, M. Alsaedi, P. Wang, *Environ. Sci. Technol.* **2018**, *52*, 5398–5406; b) X. Wang, X. Li, G. Liu, J. Li, X. Hu, N. Xu, W. Zhao, B. Zhu, J. Zhu, *Angew. Chem. Int. Ed.* **2019**, *58*, 12054–12058; *Angew. Chem.* **2019**, *131*, 12182–12186; c) H. Qi, T. Wei, W. Zhao, B. Zhu, G. Liu, P. Wang, Z. Lin, X. Wang, X. Li, X. Zhang, J. Zhu, *Adv. Mater.* **2019**, *31*, 1903378.

[7] N. Yu, R. Z. Wang, L. W. Wang, *Prog. Energy Combust. Sci.* **2013**, *39*, 489–514.

[8] Y. I. Aristov, G. Restuccia, G. Cacciola, V. N. Parmon, *Appl. Therm. Eng.* **2002**, *22*, 191–204.

[9] L. G. Gordeeva, M. M. Tokarev, V. N. Parmon, Y. I. Aristov, *React. Kinet. Catal. Lett.* **1998**, *65*, 153–159.

[10] M. J. Kalmutzki, C. S. Diercks, O. M. Yaghi, *Adv. Mater.* **2018**, *30*, 1704304.

[11] a) H. Furukawa, F. Gándara, Y. B. Zhang, J. Jiang, W. L. Queen, M. R. Hudson, O. M. Yaghi, *J. Am. Chem. Soc.* **2014**, *136*, 4369–4381; b) H. Kim, S. Yang, S. R. Rao, S. Narayanan, E. A. Kapustin, H. Furukawa, A. S. Umans, O. M. Yaghi, E. N. Wang, *Science* **2017**, *356*, 430–434; c) H. Kim, S. R. Rao, E. A. Kapustin, L. Zhao, S. Yang, O. M. Yaghi, E. N. Wang, *Nat. Commun.* **2018**, *9*, 1191.

[12] F. Fathieh, M. J. Kalmutzki, E. A. Kapustin, P. J. Waller, J. Yang, O. M. Yaghi, *Sci. Adv.* **2018**, *4*, eaat3198.

[13] a) N. Hanikel, M. S. Prévot, F. Fathieh, E. A. Kapustin, H. Lyu, H. Wang, N. J. Diercks, T. G. Glover, O. M. Yaghi, *ACS Cent. Sci.* **2019**, *5*, 1699–1706; b) R. F. Service, *Science* **2019**, *365*, 964.

[14] a) D. K. Nandakumar, S. K. Ravi, Y. Zhang, N. Guo, C. Zhang, S. C. Tan, *Energy Environ. Sci.* **2018**, *11*, 2179–2187; b) X. Zhou, F. Zhao, Y. Guo, B. Rosenberger, G. Yu, *Sci. Adv.* **2019**, *5*, eaaw5484.

[15] Y. Guo, X. Zhou, F. Zhao, J. Bae, B. Rosenberger, G. Yu, *ACS Nano* **2019**, *13*, 7913–7919.

[16] a) D. K. Nandakumar, Y. Zhang, S. K. Ravi, N. Guo, C. Zhang, S. C. Tan, *Adv. Mater.* **2019**, *31*, 1806730; b) H. Yao, P. Zhang, Y. Huang, H. Cheng, C. Li, L. Qu, *Adv. Mater.* **2019**, 1905875.

[17] R. Li, Y. Shi, M. Alsaedi, M. Wu, L. Shi, P. Wang, *Environ. Sci. Technol.* **2018**, *52*, 11367–11377.

[18] P. A. Kallenberger, M. Fröba, *Commun. Chem.* **2018**, *1*, 28.

[19] F. Zhao, X. Zhou, Y. Liu, Y. Shi, Y. Dai, G. Yu, *Adv. Mater.* **2019**, *31*, 1806446.

[20] Y. Li, H. Zhang, M. Fan, P. Zheng, J. Zhuang, L. Chen, *Sci. Rep.* **2017**, *7*, 46379.

[21] R. Li, Y. Shi, M. Wu, S. Hong, P. Wang, *Nano Energy* **2020**, *67*, 104255.

[22] a) L. Garzón-Tovar, J. Pérez-Carvajal, I. Imaz, D. Maspoch, *Adv. Funct. Mater.* **2017**, *27*, 1606424; b) A. Permyakova, S. Wang, E. Courbon, F. Nouar, N. Heymans, P. D'Ans, M. Frère, *J. Mater. Chem. A* **2017**, *5*, 12889–12898.

[23] A. LaPotin, H. Kim, S. R. Rao, E. N. Wang, *Acc. Chem. Res.* **2019**, *52*, 1588–1597.

[24] J. Y. Wang, R. Z. Wang, L. W. Wang, J. Y. Liu, *Energy* **2017**, *138*, 542–551.

[25] G. Férey, C. Mellot-Draznieks, C. Serre, F. Millange, J. Dutour, S. Surblé, I. Margiolaki, *Science* **2005**, *309*, 2040–2042.

[26] a) N. C. Burtch, H. Jasuja, K. S. Walton, *Chem. Rev.* **2014**, *114*, 10575–10612; b) C. Wang, X. Liu, N. K. Demir, J. P. Chen, K. Li, *Chem. Soc. Rev.* **2016**, *45*, 5107–5134.

[27] D. D. Wagman, W. H. Evans, V. B. Parker, R. H. Schumm, I. Halow, S. M. Bailey, K. L. Churney, R. L. Nuttall, *J. Phys. Chem. Ref. Data* **1982**, *11*, 181.

[28] Y. I. Aristov, *Appl. Therm. Eng.* **2013**, *50*, 1610–1618.

[29] a) S. Wang, J. S. Lee, M. Wahiduzzaman, J. Park, M. Muschi, C. Martineau-Corcos, A. Tissot, J. Marrot, W. Shepard, G. Maurin, J.-S. Chang, C. Serre, *Nat. Energy* **2018**, *3*, 985–993; b) A. J. Rieth, S. Yang, E. N. Wang, M. Dincǎ, *ACS Cent. Sci.* **2017**, *3*, 668–672; c) A. J. Rieth, A. M. Wright, S. Rao, H. Kim, A. D. LaPotin, E. N. Wang, M. Dinca, *J. Am. Chem. Soc.* **2018**, *140*, 17591–17596.

[30] World Health Organization, Guidelines for Drinking-Water Quality, 4th ed. **2017**.